Journal of Naval Architecture and Marine Engineering
June, 2024
http://dx.doi.org/10.3329/jname.v21i1.55428 *http://www.banglajol.info*

IMPACT OF MHD AND NANOFLUID FLOW-THROUGH A VERTICAL PLATE WITH VARYING HEAT AND MASS FLUX

M. Radhakrishnan[1], G. Palani [2*]

[1]Department of Mathematics, Sri Venkateswara College of Engineering, Sriperumbudur 602117, Tamil Nadu, India, Email: mrk@svce.ac.in
[2]Department of Mathematics, Dr. Ambedkar Govt. Arts College, Chennai 600039, Tamil Nadu, India,
[*] *Corresponding* Author's Email: gpalani32@yahoo.co.in

Abstract:

An investigation is made to discuss the effects of magnetohydrodynamic and nanofluid particles on unstable two-dimensional free convective flow through a vertical plate in the existence of heat source, radiation effect, and chemical reaction effect with varying heat and mass flux. The guiding unsteady equations were cracked using the implied finite-difference method. Here we considered four dissimilar nanofluid including Cu, Al_2O_3, TiO_2, and Ag with water as the base fluid. The flow pattern employed incorporates the result of dissimilar non-dimensional parameters for instance volume fraction, magnetic field, heat source parameter, Prandtl number, radiation effect, Schmidt number, and chemical reaction parameter. The impact of the above-mentioned parameters on the boundary layer flow characteristics (velocity, temperature, concentration, skin friction coefficient, Nusselt number, and Sherwood number) are intentional. In this study we observed that the impact of the velocity profile is maximum in silver-water nanofluid and minimum in Al_2O_3 water nanofluid but the reverse trend is observed with respect to temperature. Moreover, the outcomes are explained through graphs.

Keywords: Chemical reaction; heat source; implicit finite-difference method; magneto hydrodynamics; radiation effect.

NOMENCLATURE

$\overline{u}, \overline{v}$	dimensional fluid velocity elements in the direction of coordinate axes,$[ms^{-1}]$	$\overline{C}$	non-dimensional concentration
$\tilde{t}$	dimensional time, $[s]$	Gr	Grashof number
ν	kinematic viscosity	Gc	modified Grashof number
$\overline{T'}$	dimensional temperature of the fluid	$\overline{M}$	magnetic field parameter
$\overline{T'}_{\infty}$	dimensional temperature distant from the plate	N	buoyancy ratio parameter
$\overline{C'}$	dimensional species concentration	$\overline{Sc}$	Schmidt number
$\overline{C'}_{\infty}$	dimensional concentration in the fluid distant from the plate	$\overline{Pr}$	Prandtl number
$\overline{K'}$	dimensional chemical reaction parameter	K	dimensionless chemical reaction parameter
$\overline{D}$	species diffusion coefficient	Q	dimensionless heat source parameter
$\overline{g}$	gravitational force, ,$[m^2s^{-1}]$	R	non-dimensional radiation parameter
$\overline{c}_p$	heat capacitance	**Greek symbols**	
$\overline{k}$	heat conductivity of the fluid,$[Wm^{-1}K^{-1}]$	$\overline{\rho}$	fluid density
μ	coefficient of viscosity	σ	electrical conductivity of the fluid
$\overline{X}, \overline{Y}$	dimensionless coordinates over and normal to the plate	$\overline{\beta}$	volumetric coefficient of expansion
L	length of the plate	**Subscripts**	
$\overline{U}, \overline{V}$	dimensionless velocity components along x, y-axes	∞	free stream conditions
$\overline{t}$	non-dimensional time	$\overline{f}, \overline{s}$	thermo-physical features of water and solid nanoparticle

1813-8535 (Print), 2070-8998 (Online) Received on: Sept., 2021

$\overline{T}$	non-dimensional temperature	$\overline{nf}$	thermo-physical features of the nanofluid

1. Introduction

In recent years the mixed impacts of thermal and mass transport in nanofluid particles have been a subject of great importance in science and engineering. The word "nanofluid" created by Choi (1995) characterizes a fluid suspension that consists of the finest molecules (radius < 25 nm). The finest molecules are commonly built by a great efficiency pulsed method from a conductive material. Several methods were suggested to interpret the improved thermal transport traits of nanofluid. Natural convection flows around vertical bodies, known for their instability, play a crucial role in both scientific research and engineering applications. These flows are frequently utilized to enhance heat transfer around various electrical and electronic devices, including nuclear reactors. Additionally, heat transfer is of paramount importance in manufacturing processes such as heat extrusion, metal forming, and crystal growing (Rajesh et al., 2016). In the realm of biomedical engineering, nanofluid are employed in a variety of applications including microelectronics, microfluidics, transportation, X-ray technology, material processing, and scientific instrumentation (Veera Krishna, M. and Ali J., 2020).

For instance, Aziz and Khan (2012) reported a transient free convectively heated vertical plate over a nanofluid flow. Marneni Narahari (2018) attributed numerically the nanofluid flow over a semi-infinite plate with constant thermal flux. Radiation effects on nanofluid past a vertically accelerated plate with varying wall temperature have been presented by Astutia *et al* (2019). Irfan Mustafa and Tariq Javed (2019) investigated thermal transport in the inherent advection flow of nanofluid with a vertical wavy plate with varying thermal flux. Mondal *et al* (2019) bestowed a 2-D nanofluid flow because of the mixed results of thermal and mass diffusion. Moreover, Mishra *et al*(2020) have discussed the results of EG (Ethylene–Glycol) based nanofluid past a semi-infinite plate over a porous channel. Khatun, S., and Nasrin, R. (2021) explored numerical modeling of Buongiorno's nanofluid, emphasizing free convection incorporating thermophoresis and Brownian motion effects. Recently, Swain, B. K., et al. (2023) conducted a study on heat transfer, focusing on viscous dissipation and entropy generation in a nanofluid flow through a porous medium. The governing equations were solved using similarity transforms technique.

The analyses of MHD flow have vital utilization in science and engineering. Mechanical apparatus, namely MHD dynamo, pumps, and bearings are concerned with the interplay between electro conductive liquid and magnetic strength. MHD frontier laminas are detected in varied mechanical methods engaging molten iron and blood flow crosswise of magnetic strength. Ali J. Chamkha et al. (2002) have analyzed numerically the problem of natural convection about a vertical plate in porous media. Chamkha and Aly (2011) presented the effects of MHD and nanofluid flow past a vertical plate with thermal sources. An exact result of emission impacts on MHD and nanofluid flow past a moving vertical plate has been investigated by Das and Jana (2015). Loganathan *et al*(2015) examine an unstable MHD free convective flow of water-based nanofluid particles over a vertical plate with a radiation effect. The study of unsteady MHD flow and thermal transport of nanofluid along an impulsively initiated semi-infinite vertical plate were presented by Rajesh *et al*(2016). Hari *et al*(2017) explained the flow characteristics investigation of gravity-driven convective nanofluid flow in a porous medium over an oscillating plate in the existence of MHD. Macha Madhu et al. (2017)examined the impact of heat radiation on MHD flow of Maxwell fluid over a stretching sheet. The analytical solution of combined thermal and mass transfer consequences on MHD water-based nanofluid movement through an inclined plate has been examined by Palani *et al*(2018). The effects of normally applied magnetic strength on the vertical plate over a Casson fluid flow have been presented numerically using the Runge-Kutta method with the shooting technique by Parandhamaa *et al*(2019). MHD flow of a Casson fluid in a vertical plate taking into cognizance the chemical absorption effect was discussed recently by Omokhuale Emmanuel *et al*(2020). Parida, B. C., et al. (2021) examined the effects of mass transfer on viscous dissipative MHD flow of a nanofluid over a stretching sheet embedded in a porous medium.

In the published articles, nobody has conveyed until now the study of the collective effect of radiation and chemical reaction in transient free two-dimensional (2-D) MHD convection nanofluid flow over a vertical plate with heat generation and varying heat and mass fluxes. We extended the work of Loganathan *et al.* (2015) and with the novelty of considering heat source, chemical reaction effect and mass transfer in nanofluid. The purpose in the present examination is to analyze the importance of various values of the material parameters not

only on fluid characteristics but also the Nusselt number, skin friction, and the shear stress. Such a study is found useful for nonmaterial's heat transport processing in the metallurgy and chemical engineering.

2. Mathematical Analysis

Here we have considered an unstable 2-D free convective nanofluid flow through an immense vertical plate with an applied magnetic induction. In the coordinate system, we have considered the x'-axis to be ahead of the plate in the upright (vertical) order, and the y'-axis is considered orthogonal to the plate. The gravitational force $\overline{g}$ operates towards the bottom. At $\tilde{t} \leq 0$, the temperature of the plate and the nanofluid are in an equilibrium position. When time $\tilde{t} > 0$, the temperature and the concentration flatten adjacent to the plate are elevated evenly. We assume that the emission effect and the thermal and mass fluxes to be implemented, parallel to the y'- axis. A consistent crosswise magnetic induction of magnitude B_0^2 is applied orthogonal to x'-axis. We have hypothetical that the concentration of the disseminating species in the two fold combination was extremely tiny in resemblance with another present chemical species. The fluid considered in this study is a water-based nanofluid that includes four classes of spherical shape nanoparticles Ag, Cu, Al_2O_3 and TiO_2 whose thermo-physical characteristics (Loganathan *et al*.2015; Rajesh *et al*.2016) are given in Table1. Besides, it is expected that the pure fluid (water) and the suspended nanofluid molecules are in thermal balance. The governing unsteady momentum, thermal energy, and mass diffusion equations in accordance with the model for nanofluid presented by Chamkha *et al* (2011) and Loganathan *et al*(2015) fulfilling Boussinesq approximation (Schlichting, 2001) in the existence of magnetic field, emission (radiation), and chemical reaction in spatial form could be stated as:

$$\frac{\partial \overline{u}}{\partial x'} + \frac{\partial \overline{v}}{\partial y'} = 0 \tag{1}$$

$$\frac{\partial \overline{u}}{\partial \tilde{t}} + \overline{u}\frac{\partial \overline{u}}{\partial x'} + \overline{v}\frac{\partial \overline{u}}{\partial y'} = \frac{\overline{(\rho\beta)}_{\overline{nf}}}{\overline{\rho}_{\overline{nf}}}\overline{g}\left[(\overline{T'} - \overline{T'}_{\infty}) + (\overline{C'} - \overline{C'}_{\infty})\right] + \overline{v}_{\overline{nf}}\frac{\partial^2 \overline{u}}{\partial y'^2} - \frac{\sigma B_0^2 \overline{u}}{\overline{\rho}_{\overline{nf}}} \tag{2}$$

$$\frac{\partial \overline{T'}}{\partial \tilde{t}} + \overline{u}\frac{\partial \overline{T'}}{\partial x'} + \overline{v}\frac{\partial \overline{T'}}{\partial y'} = \frac{1}{\overline{(\rho C_p)}_{\overline{nf}}}\left[\overline{k}_{\overline{nf}}\frac{\partial^2 \overline{T'}}{\partial y'^2} - \frac{\partial \overline{q}_{\overline{r}}}{\partial y'} + \overline{Q'}(\overline{T'} - \overline{T'}_{\infty})\right] \tag{3}$$

$$\frac{\partial \overline{C'}}{\partial \tilde{t}} + \overline{u}\frac{\partial \overline{C'}}{\partial x'} + \overline{v}\frac{\partial \overline{C'}}{\partial y'} = \overline{D}\frac{\partial^2 \overline{C'}}{\partial y'^2} - \overline{K'}(\overline{C'} - \overline{C'}_{\infty}) \tag{4}$$

The dimensional form of boundary conditions are taken to be,

$$\left\{\begin{array}{c} \tilde{t} \leq 0: \overline{u} = 0, \quad \overline{v} = 0, \quad \overline{T'} = \overline{T'}_{\infty}, \quad \overline{C'} = \overline{C'}_{\infty} \quad \forall\, x' and\, y \\ \tilde{t} > 0: \overline{u} = 0, \quad \overline{v} = 0, \quad \dfrac{\partial \overline{T'}}{\partial y'} = -\left[\dfrac{\overline{q}_{\overline{w}}(x')}{\overline{k}}\right], \dfrac{\partial \overline{C'}}{\partial y'} = -\left[\dfrac{\overline{q}^*_{\overline{w}}(x')}{\overline{D}}\right] \; at\; y' = 0 \\ \overline{u} = 0, \;\; \overline{v} = 0, \overline{T'} = \overline{T'}_{\infty}, \;\; \overline{C'} = \overline{C'}_{\infty} \;\; at\; x' = 0 \\ \overline{u} \to 0, \;\; \overline{v} \to 0, \overline{T'} \to \overline{T'}_{\infty}, \;\; \overline{C'} \to \overline{C'}_{\infty} \;\; at\; y' \to 0 \end{array}\right\} \tag{5}$$

where $\overline{q}_{\overline{w}}(x') = \overline{a}x'^{m}$ and $\overline{q}^*_{\overline{w}}(x') = \overline{b}x'^{m}$

Table 1: Thermo-physical characteristics of nanoparticles

Physical features	Water (H_2O)	Copper (Cu)	Aluminum Oxide (Al_2O_3)	Titanium Dioxide (TiO_2)	Silver (Ag)
$\overline{\rho}(kg/m^3)$	997.10	8933.0	3970.0	4250.0	10500.0
$\overline{C_p}(J/kgK)$	4179.0	385.0	765.0	686.2	235.0
$\overline{k}(W/mK)$	0.613	401.0	40.0	8.9538	429.0
$\overline{\beta} \times 10^{-5}(K^{-1})$	21.0	1.67	0.85	0.90	1.89

This paper deals with a spherical-shaped nanoparticles with heat conduction and dynamic viscidity. For nanofluid (fluid containing spherical nanoparticles), the equations of effective dynamic viscosity $\overline{\mu}_{\overline{nf}} = \dfrac{\overline{\mu}_{\overline{f}}}{(1-\overline{\phi})^{2.5}}$, density $\overline{\rho}_{\overline{nf}} = (1-\overline{\phi})\overline{\rho}_{\overline{f}} + \overline{\phi}\overline{\rho}_{\overline{s}}$, thermal capacitance

$(\overline{\rho c_p})_{\overline{nf}} = (1-\overline{\phi})(\overline{\rho c_p})_{\overline{f}} + \overline{\phi}(\overline{\rho c_p})_{\overline{s}}$, thermal and mass expansion coefficient $(\overline{\rho\beta_T})_{\overline{nf}} = (1-\overline{\phi})(\overline{\rho\beta_T})_{\overline{f}} + \overline{\phi}(\overline{\rho\beta_T})_{\overline{s}}, (\overline{\rho\beta_C})_{\overline{nf}} = (1-\overline{\phi})(\overline{\rho\beta_C})_{\overline{f}} + \overline{\phi}(\overline{\rho\beta_C})$ and effective heat conductivity $\frac{\overline{k}_{\overline{eff}}}{\overline{k}_{\overline{f}}} = \frac{\overline{k}_{\overline{s}} + 2\overline{k}_{\overline{f}} - 2\overline{\phi}(\overline{k}_{\overline{f}} - \overline{k}_{\overline{s}})}{\overline{k}_{\overline{s}} + 2\overline{k}_{\overline{f}} + \overline{\phi}(\overline{k}_{\overline{f}} - \overline{k}_{\overline{s}})}$ are proposed by (Das *et al*, 2015, Loganathan *et al*, 2015, , Rajesh *et al*, 2016, Palani *et al*, 2018 and Hamilton and Crosser,1962).

On introducing the relevant non-dimensional quantities are

$$\left\{\begin{array}{c} \overline{X} = \frac{x'}{L}, \quad \overline{Y} = \frac{y'}{L}Gr^{\frac{1}{4}}, \quad \overline{U} = \frac{\overline{u}L}{\nu_{\overline{f}}}Gr^{-\frac{1}{2}}, \quad \overline{V} = \frac{\overline{v}L}{\nu_{\overline{f}}}Gr^{-\frac{1}{4}}, \quad t = \frac{\nu_{\overline{f}}\tilde{t}}{L^2}Gr^{\frac{1}{2}}, \\ \overline{T} = \frac{\overline{k}[T' - T'_\infty]}{\overline{q}_{\overline{w}}(L)L}Gr^{\frac{1}{4}}, \quad \overline{C} = \frac{\overline{D}[C' - C'_\infty]}{\overline{q}^*_{\overline{w}}(L)L}Gr^{\frac{1}{4}}, \quad \overline{Pr} = \frac{\mu\overline{C}_p}{\overline{k}_{\overline{f}}} \\ Gr = \frac{\overline{(g\beta_T)}_{\overline{f}}L^4\overline{q}_{\overline{w}}(L)}{\nu^2_{\overline{f}}k_{\overline{f}}}, Gc = \frac{\overline{(g\beta_C)}_{\overline{f}}L^4\overline{q}^*_{\overline{w}}(L)}{\nu^2_{\overline{f}}\overline{D}_{\overline{f}}}, \overline{M} = \frac{\sigma B_0^2 L^2}{\mu_{\overline{f}}}Gr^{-\frac{1}{2}}, Q = \frac{\overline{Q'}L^2}{\nu_{\overline{f}}\overline{(\rho C_p)}_{\overline{f}}}Gr^{-\frac{1}{2}}, \\ \overline{Sc} = \frac{\nu_{\overline{f}}}{\overline{D}}, N = \frac{Gc}{Gr}, K = \frac{\overline{K'}L^2}{\nu_{\overline{f}}}Gr^{-\frac{1}{2}}, \nu_{\overline{f}} = \frac{\mu_{\overline{f}}}{\overline{\rho}_{\overline{f}}}, R = \frac{16a^*\sigma\overline{T}^3_\infty L^2}{k_{\overline{f}}}Gr^{-\frac{1}{2}} \end{array}\right\} \quad (6)$$

Taking the Rosseland approximation (Brewster, 1992**)**, induce the radiation thermal flux:

$q_r = \frac{4\overline{\sigma}^*}{3\overline{k}^*}\frac{\partial}{\partial y'}(\overline{T'}^4)$, here $\overline{\sigma}^*$ stand for Stefan-Boltzmann constant, and $\overline{k}^*$ is the average absorption coefficient.

$$\frac{\partial}{\partial y'}(q_r) = -4\overline{a}^*\overline{\sigma}^*(\overline{T'}^4_\infty - \overline{T'}^4) \quad (7)$$

Using Taylor's expansion method, expand $\overline{T'}^4$ over $\overline{T'}_\infty$ leads to

$$\overline{T}^4 \cong (4\overline{T}^3_\infty)\overline{T} - 3\overline{T}^4_\infty \quad (8)$$

Then equations (1) to (4) in view of equations (5) to (8), and the above assumptions reduced as:

$$\frac{\partial}{\partial\overline{X}}(\overline{U}) + \frac{\partial}{\partial\overline{Y}}(\overline{V}) = 0 \quad (9)$$

$$\frac{\partial\overline{U}}{\partial\overline{t}} + \overline{U}\frac{\partial\overline{U}}{\partial\overline{X}} + \overline{V}\frac{\partial\overline{U}}{\partial\overline{Y}} = \frac{1}{\left(1-\overline{\phi}\right) + \overline{\phi}\left(\frac{\overline{\rho}_{\overline{s}}}{\overline{\rho}_{\overline{f}}}\right)}\left\{\begin{array}{c} \left[\left(1-\overline{\phi}\right) + \overline{\phi}\frac{\overline{(\rho\beta)}_{\overline{s}}}{\overline{(\rho\beta)}_{\overline{f}}}\right]Gr^{-\frac{1}{4}}\overline{T} + \\ \left[\left(1-\overline{\phi}\right) + \overline{\phi}\frac{\overline{(\rho\beta)}_{\overline{s}}}{\overline{(\rho\beta)}_{\overline{f}}}\right]Gr^{-\frac{1}{4}}N\,\overline{C} + \\ \frac{1}{\left(1-\overline{\phi}\right)^{2.5}}\frac{\partial^2\overline{U}}{\partial\overline{Y}^2} - \overline{MU} \end{array}\right\} \quad (10)$$

$$\frac{\partial\overline{T}}{\partial\overline{t}} + \overline{U}\frac{\partial\overline{T}}{\partial\overline{X}} + \overline{V}\frac{\partial\overline{T}}{\partial\overline{Y}} = \frac{1}{(1-\overline{\phi}) + \overline{\phi}\left(\frac{\overline{(\rho C_p)}_{\overline{s}}}{\overline{(\rho C_p)}_{\overline{f}}}\right)}\left[\frac{\overline{k}_{\overline{nf}}}{\overline{k}_{\overline{f}}}\frac{1}{\overline{Pr}}\frac{\partial^2\overline{T}}{\partial\overline{Y}^2} - \frac{1}{\overline{Pr}}R\overline{T} + Q\overline{T}\right] \quad (11)$$

$$\frac{\partial\overline{C}}{\partial\overline{t}} + \overline{U}\frac{\partial\overline{C}}{\partial\overline{X}} + \overline{V} = \frac{1}{\overline{Sc}}\frac{\partial^2\overline{C}}{\partial\overline{Y}^2} - K\overline{C} \quad (12)$$

Eq. (5) using Eq. (6) can be written in a dimensionless form as:

$$\left.\begin{array}{c} \overline{t} \le 0: \overline{U} = 0,\ \overline{V} = 0,\ \overline{T} = 0,\ \overline{C} = 0 \quad for\ all\ \overline{X}\ and\ \overline{Y} \\ \overline{t} > 0: \overline{U} = 0,\ \overline{V} = 0,\ \frac{\partial}{\partial \overline{Y}}(\overline{T}) = -\overline{X}^{n},\ \frac{\partial}{\partial \overline{Y}}(\overline{C}) = -\overline{X}^{m}\ at\ \overline{Y} = 0 \\ \overline{U} = 0,\ \ \overline{T} = 0,\ \overline{C} = 0 \quad at\ \overline{X} = 0 \\ \overline{U} \to 0,\ \ \overline{T} \to 0,\ \overline{C} \to 0 \quad as\ \overline{Y} \to \infty \end{array}\right\} \tag{13}$$

For engineering purposes, the dimensionless form of local as well as mean Nusselt number, skin friction, and Sherwood number are presented as follows:

$$Nu_{\overline{X}} = -\frac{\overline{k}_{\overline{nf}}}{\overline{k}_{\overline{f}}}\overline{X}Gr^{\frac{1}{4}}\left(\frac{\partial \overline{T}}{\partial \overline{Y}}\right)_{\overline{Y}=0} / \overline{T}_{\overline{Y}=0}$$

$$\overline{Nu} = -\frac{\overline{k}_{\overline{nf}}}{\overline{k}_{\overline{f}}}Gr^{\frac{1}{4}}\int_0^1 \left[\frac{\left(\frac{\partial \overline{T}}{\partial \overline{Y}}\right)_{\overline{Y}=0}}{\overline{T}_{\overline{Y}=0}}\right] d\overline{X}$$

$$\tau_{\overline{X}} = \frac{1}{(1-\overline{\phi})^{2.5}}Gr^{3/4}\left(\frac{\partial \overline{U}}{\partial \overline{Y}}\right)_{\overline{Y}=0}$$

$$\overline{\tau} = \frac{1}{(1-\overline{\phi})^{2.5}}Gr^{3/4}\int_0^1 \left(\frac{\partial \overline{U}}{\partial \overline{Y}}\right)_{\overline{Y}=0} d\overline{X}$$

$$Sh_{\overline{X}} = -Gr^{1/4}\left(\frac{\partial \overline{C}}{\partial \overline{Y}}\right)_{\overline{Y}=0}$$

$$\overline{Sh} = -Gr^{1/4}\int_0^1 \left(\frac{\partial \overline{C}}{\partial \overline{Y}}\right)_{\overline{Y}=0} d\overline{X}$$

3. Solution Procedure

The dimensionless form of governing equations (9)-(12) with appropriate initial and boundary conditions Eq. (13) is cracked numerically by engaging well organized and unconditionally stable method namely Crank-Nicolson Method. For calculation purposes, we think through the area of integration as a rectangle with edges $\overline{X}_{max}(= 1.0)$ and $\overline{Y}_{max}(= 16.0)$. Here, $\overline{Y}_{max}$ refers $\overline{Y} = \infty$ that situated good enough exterior of the velocity, thermal, and concentration boundary layers. Subsequently, some preliminary investigation was carried out to choose the maximum value of $\overline{Y}$ which satisfies the last two boundary conditions (13). The grid size was chosen as $\Delta\overline{X} = 0.05,\ \overline{Y} = 0.25$ and $\Delta\overline{t} = 0.01$ for calculation purposes. The computational process was carried out till it reached a stable position and tolerance limit was fixed as 10^{-5}. The offered method is compatible as well as absolutely stable which declares that the scheme is convergent.

4. Discussion of Results

For a clear understanding of the flow problem, the effects of numerous values of the parameters on $\overline{U}, \overline{T}$ and $\overline{C}$ contours are calculated numerically and the outcomes are illustrated diagrammatically. We examine four kinds of water-based nanofluid including Cu, Al_2O_3, TiO_2, and Ag nanoparticles for analysis. Since accumulation occurs when the volume fraction $(\overline{\phi})$ of nanoparticles exceed 8%, we choose $\overline{\phi}$ as $0 \le \overline{\phi} \le 0.04$. When $\phi = 0$ our analysis is scaled down to normal fluid.

Effects of unsteady and steady-state velocity and temperature contours for different Cu, Al_2O_3, TiO_2, and Ag water-based nanofluid and base fluid as fixed values of different parameters are depicted respectively in Fig.1 and Fig. 2. It is identified from Fig. 1 that the velocity profile is utmost for silver water (Ag) among the nanofluid but least in Al_2O_3 water nanofluid. But the reversal effect is found far away from the plate. Further, we observed that as time increases as velocity decreases. But in Fig. 2, we noted that the temperature profile attains the highest for Al_2O_3 water among the considered nanofluid but reaches the lowest for Ag water nanofluid. When time increases with an increase in the temperature is also found. Finally, it is seen that the effect of the

velocity of water decreases in comparison with nanofluid considered in this study. But the reverse trend is observed with respect to temperature.

The impact of TiO_2 water nanofluid on transient and steady-state velocity and temperature contour as several values of magnetic parameter $\overline{M}$ is presented graphically in Fig. 3 and Fig. 4. It can be recognized from Fig. 3 the velocity of the titanium dioxide water nanofluid reduces as $\overline{M}$ and time upsurges. The effect of magnetic force on an electro-conductive liquid induces a resistant kind of strength named Lorentz force. The transport of the fluid in the boundary layer is diminishing due to this force. This induces the velocity contour of TiO_2 water nanofluid possess to a distinct maximum very close to the plate but as $\overline{M}$ upsurges the above-mentioned maximum reduces and progresses evenly in the free stream.

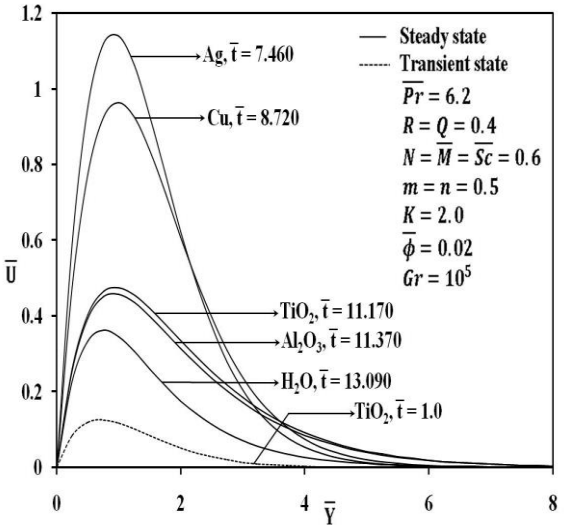

Fig.1 Velocity distribution for different nano particles

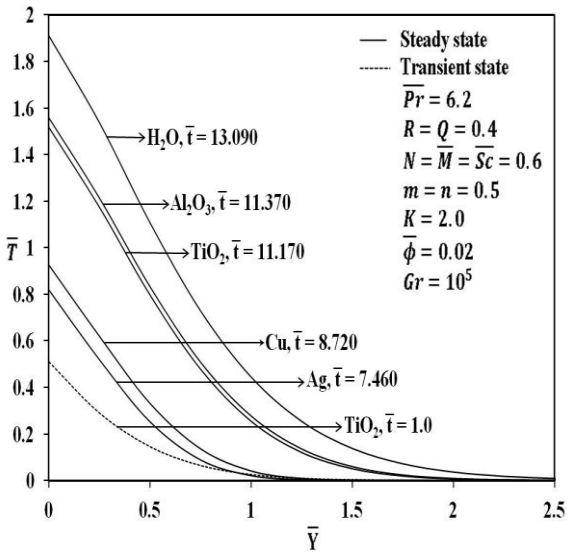

Fig.2 Temperature distribution for different nano particles

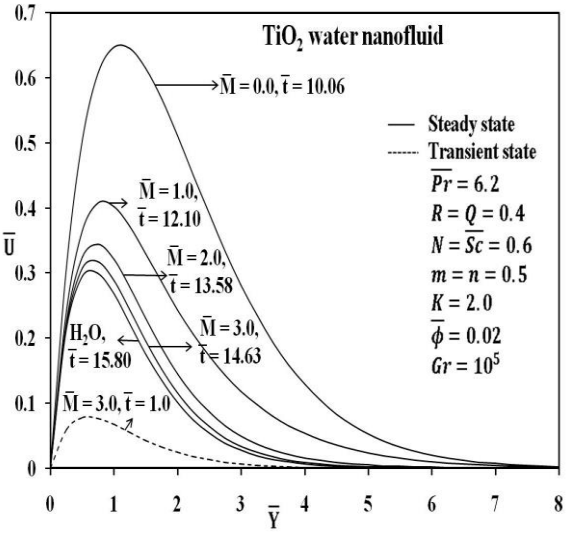

Fig.3 Velocity distribution for differnt $\overline{M}$

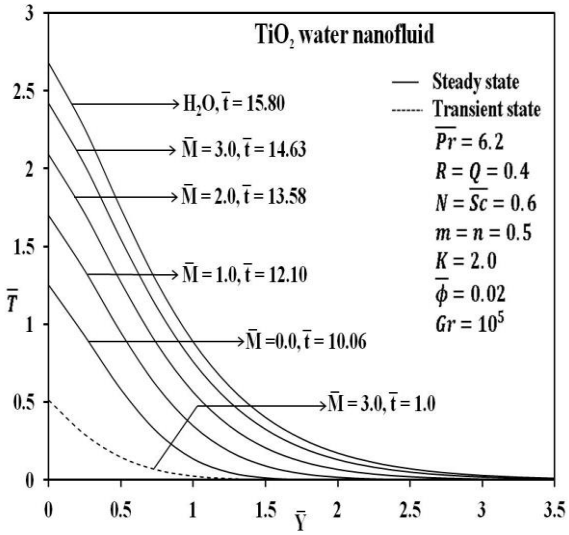

Fig. 4 Temperature distribution for different $\overline{M}$

The development of water-based copper nanofluid momentum and energy profiles for various quantities of R is exhibited in Fig. 5 and Fig. 6. As seen from Fig. 5, the velocity of the fluid upsurges with the decrease in R but upsurges with time, until the value of $\overline{Y} \leq 1$ and an opposite trend is observed at $\overline{Y} = 1.75$. The velocity contour that water-based copper nanofluid exhibits is larger compared to water. Fig. 6 shows the temperature

profile for water-based copper nanofluid increases as R decreases. Additionally, the temperature of the water is greater than Cu-water nanofluid at $R = 2.0$.

Fig.7 and Fig.8 are graphed to analyze the influence of heat source parameter Q on transient and steady-state velocity and temperature profiles for Al_2O_3-water nanofluid. As expected, the stable state velocity and temperature profile significantly increase as the heat source parameter increases with time. Also, it can be seen from those graphs that the stable state velocity profile of base fluid is lower compared with Al_2O_3-water nanofluid at $Q = 0.6$ but an opposite progress is observed with respect to temperature.

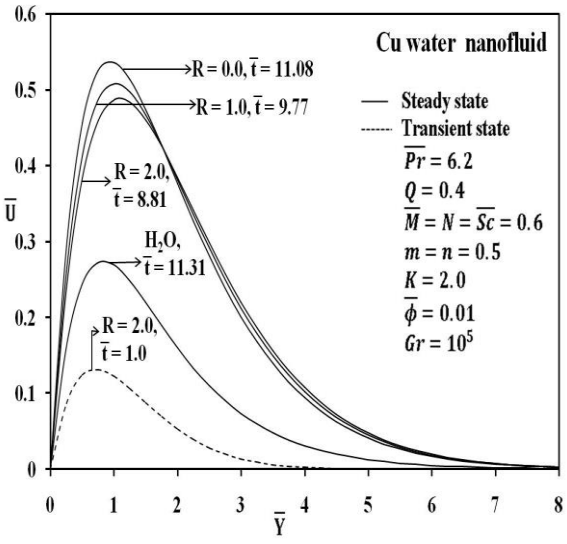

Fig. 5 Velocity distribution for differnt R

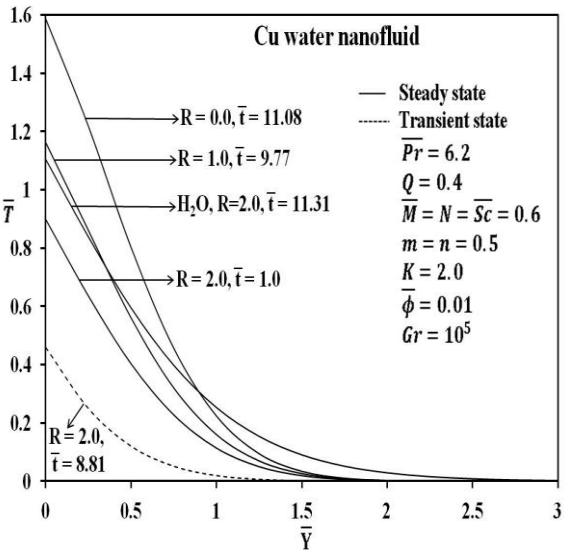

Fig.6 Temperature distribution for different R

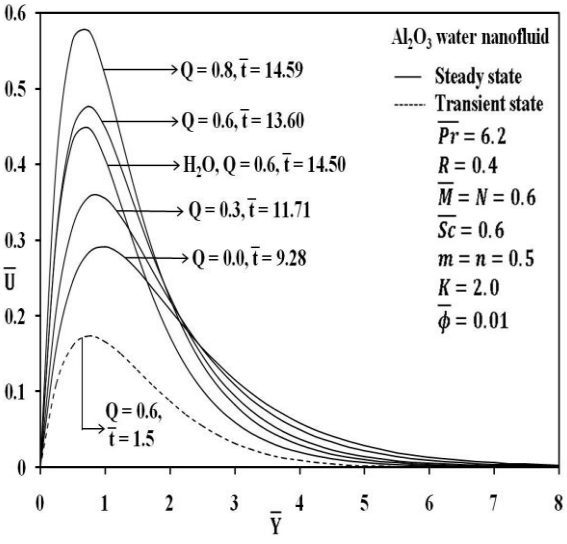

Fig. 7 Velocity distribution for different Q

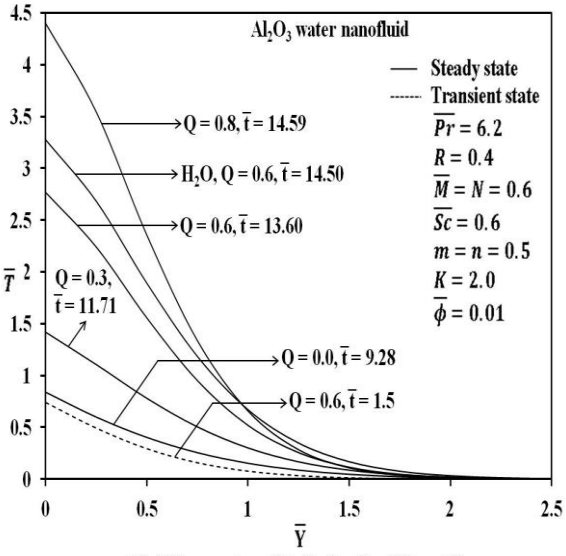

Fig.8 Temperature distribution for different Q

The nature of unsteady, steady, and temporal maximum velocity, temperature, and concentration contours in the water-based Ag-nanofluid under the impact of destructive ($K > 0$) and generative ($K < 0$) chemical reaction parameter K is presented in Figs. 9-11. It can be observed from Fig. 9 and Fig. 11 that the steady-state velocity and concentration profiles tend to decrease as K decreases but a reversal effect is realized with respect to the temperature profile as seen in Fig. 10. In addition, the temporal maximum is noticed for velocity, temperature,

and concentration contours respectively at the time $\bar{t} = 1.80$. Furthermore, steady-state velocity profiles for base fluid is reduced in correlation with Ag-water nanofluid but it is greater in steady-state temperature.

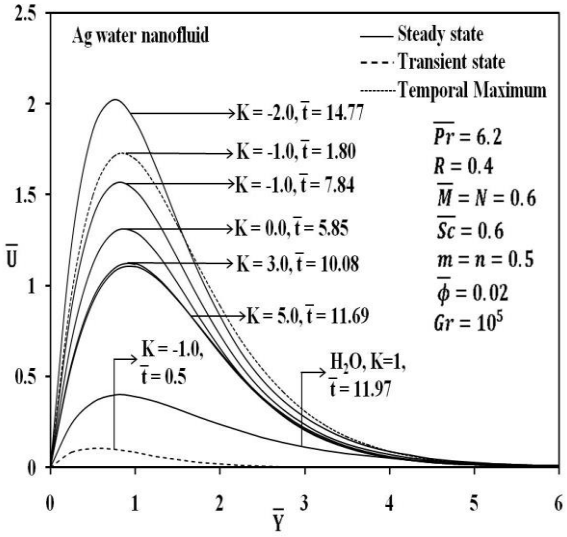

Fig. 9 Velocity distribution for different K

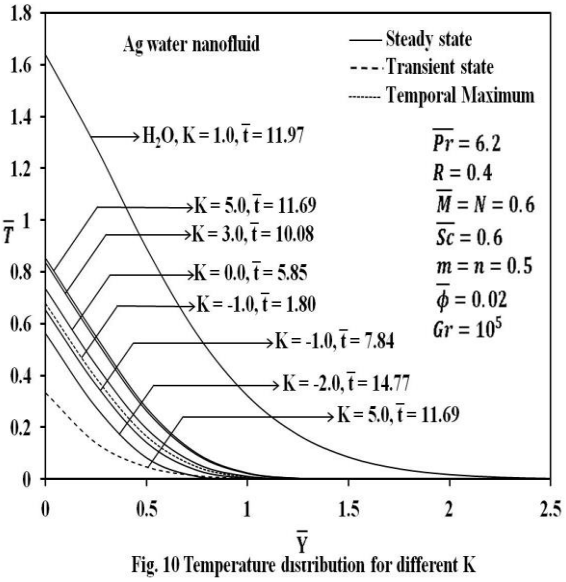

Fig. 10 Temperature distribution for different K

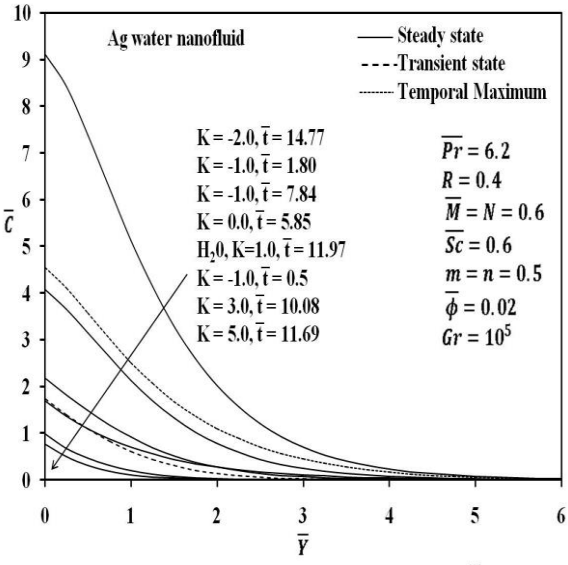

Fig. 11 Concentration distribution for different $\bar{C}$

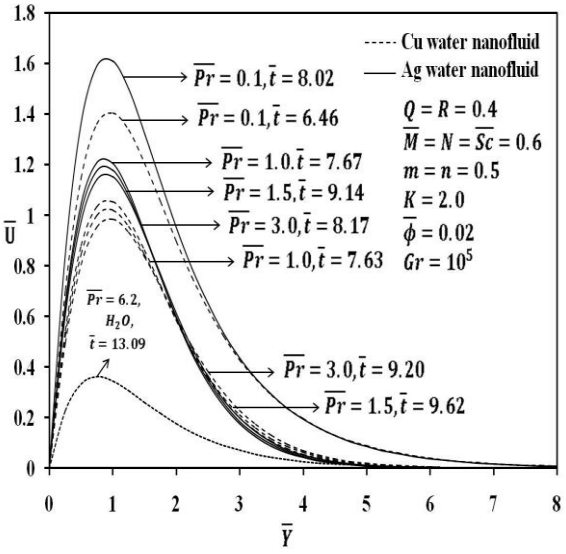

Fig.12 Steady state velocity distribution for different $\overline{Pr}$

Fig.12 and Fig.13 presented the analogy of stable condition velocity and temperature profiles for distinct values of the Prandtl number $\overline{Pr}$ for copper and silver-water nanofluid. These graphs reported that the velocity and temperature of the fluid (nano) upsurges as $\overline{Pr}$ decreases because the fluid with high $\overline{Pr}$ values has indeed higher adhesive, that upsurges the momentum and heat boundary-layer density, because of this, diminishes the flow velocity including the temperature of the fluid. It is also noticed that the steady-state Ag-water nanofluid non-dimensional velocity profile is higher than Cu-water nanofluid and reversal result is noticed to be distant from the plate. Besides, it can be seen that the temperature of copper-water nanofluid elevated compared to Ag-water nanofluid, this is because of the elevated thermal conductivity of Cu-water nanofluid.

Fig.14 and Fig.15 reveal the steady-state velocity and temperature variations of silver and copper water-based nanofluid in the simultaneous absence and presence of $\overline{\phi}$. It is perceived that the steady-state velocities of silver and copper water based nanofluid are increases with $\overline{\phi}$. This is happening because of the rise in the values of $\overline{\phi}$

gives rise to the density of the velocity boundary layer. Also, it is noticed that the momentum of copper-water nanofluid is lower than silver-water nanofluid. But the converse effect is observed in the case of steady-state temperature with respect to $\overline{\phi}$. Furthermore, the time to attain the stable state temperature is higher compared with steady-state velocity. In addition, the velocity of water diminishes compared with Ag-water and Cu-water nanofluid but an opposite effect is registered in temperature.

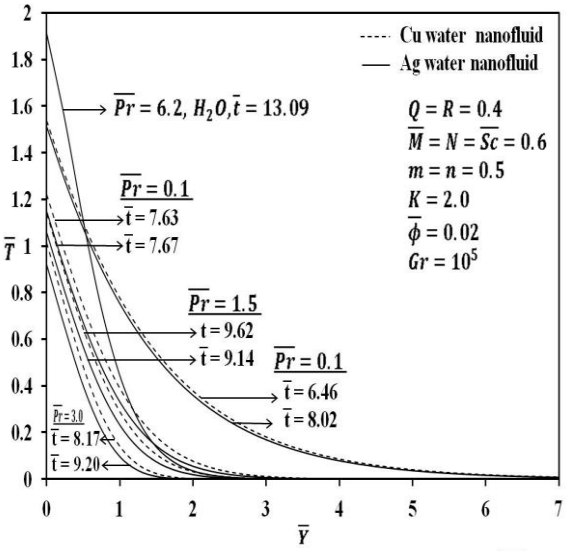

Fig.13 Steady state temperature distribution for different $\overline{Pr}$

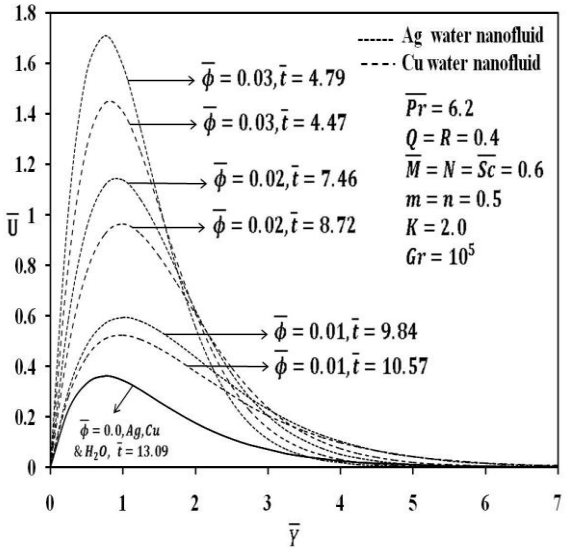

Fig.14 Steady state velocity distribution for different $\overline{\phi}$

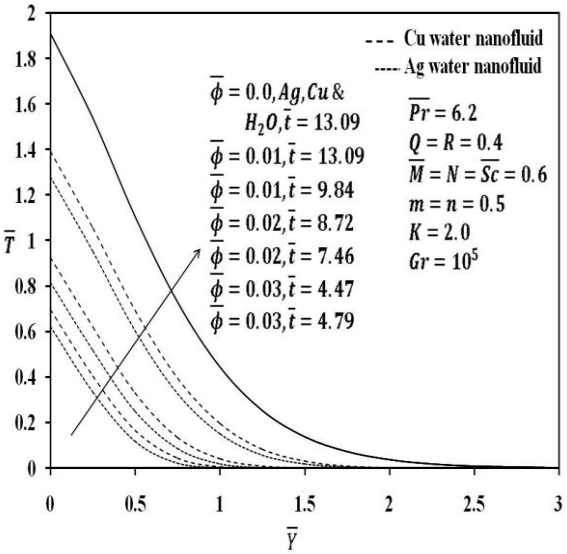

Fig.15 Steady state temperature distribution for different $\overline{\phi}$

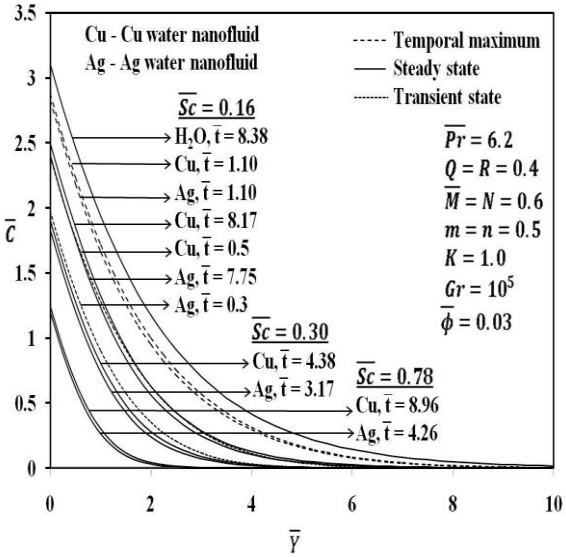

Fig. 16 Concentration distribution for different $\overline{Sc}$

Fig.16 underline the effect of $\overline{Sc}$ on concentration, profile reveals that the increment in $\overline{Sc}$ induces the reduction in concentration for copper and silver water nanofluid. Also, it is clear that the concentration attributed to copper-water nanofluid is higher than silver-water nanofluid. Moreover, the water shows a greater concentration contour than nanofluid.

It can be observed based on Fig. 17 and Fig. 20 that the local and average Nusselt number ($Nu_{\overline{X}}$ and $\overline{Nu}$) escalates almost geodesic line away from the plate for Ag water-based nanofluid. In addition, we noticed that the local and average Nusselt number increases as R, varying mass flux exponent (m) and varying heat flux exponent (n) rises but diminishes with an increment in $\overline{M}$ and K for the fixed value of $Q = 0.6$.

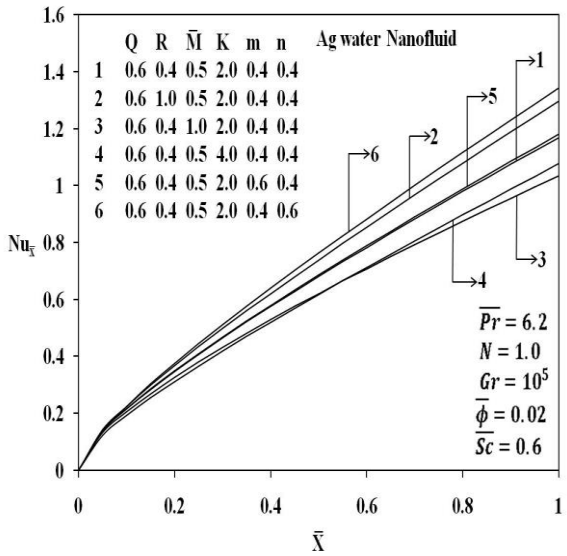

Fig. 17 Local Nusselt number

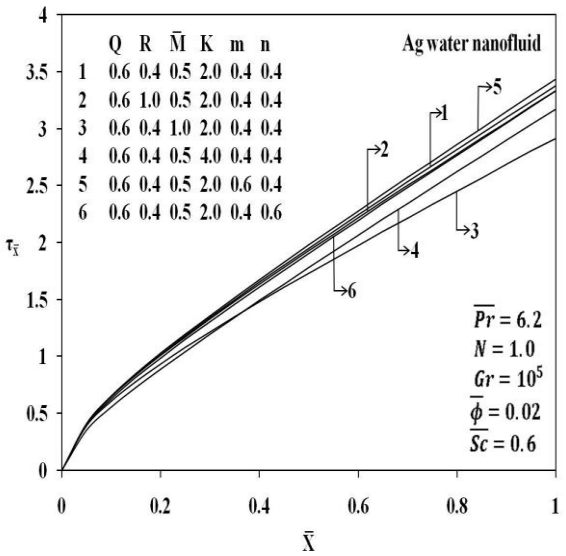

Fig.18 Local Skinfriction

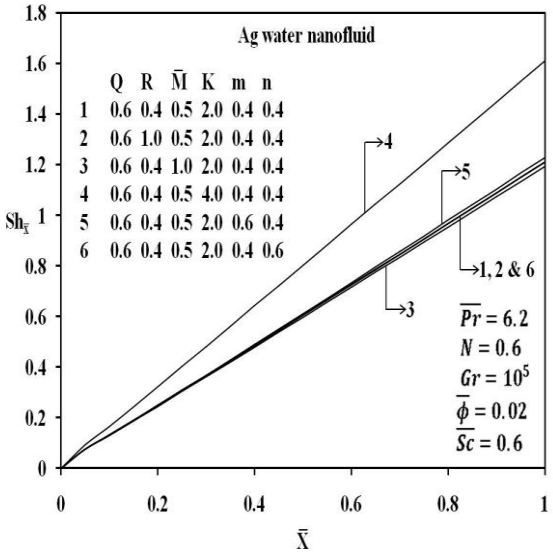

Fig.19 Local Sherwood number

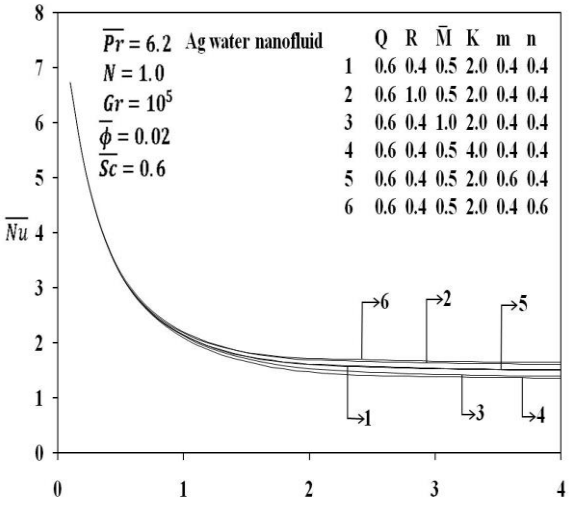

Fig. 20 Average Nusselt number

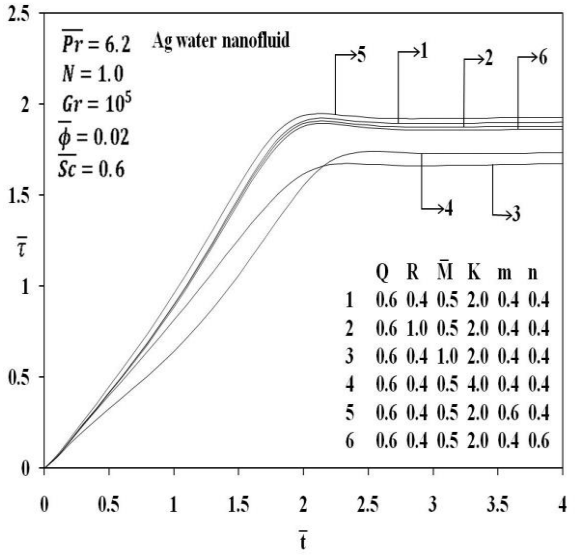

Fig. 21 Average Skin friction

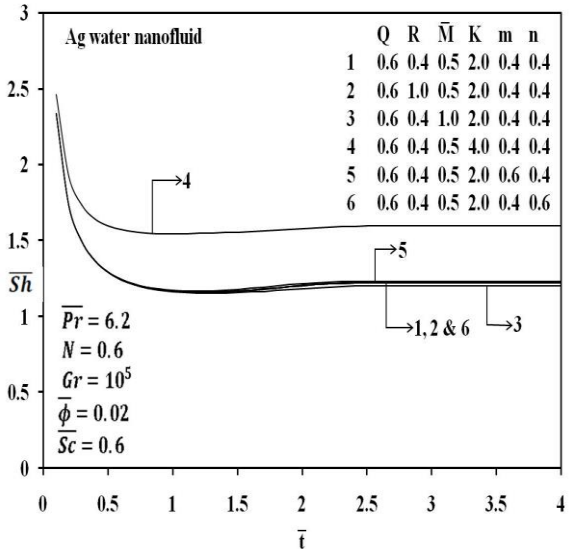

Fig. 22 Average Sherwood number

The variation of $\tau_{\overline{X}}$(local skin friction) and $\overline{\tau}$(average skin friction) coefficient against $R, \overline{M}, K, m$ and n on Ag water-based nanofluid for the fixed value of $Q = 0.6$ is presented in Fig. 18 and Fig. 21. From these graphs, we declared the coefficient of $\tau_{\overline{X}}$ and $\overline{\tau}$ reduce as $R, \overline{M}, K, m$ and n rise but we have seen an enhanced effect in $\tau_{\overline{X}}$ and $\overline{\tau}$ coefficient with a raise in varying heat flux exponent(n).

Fig.19 and Fig.22 illustrated the influence of local and average Sherwood number for Ag water-based nanofluid with changes in the values of $R, \overline{M}, K, m$ and n for the fixed value of $Q = 0.6$. We are aware from these graphs that the result of increasing $K$and m enhance the local and average Sherwood number. However, a reverse trend is noted for $\overline{M}$.

5. Conclusions

We have summarized following comments:

- The velocity profile is observed to be highest in silver-water nanofluid and lowest in Al_2O_3-water nanofluid among the nanofluid considered in this study but the reverse trend is observed with respect to temperature.
- As expected, $\overline{M}$ upsurges with time, the titanium dioxide water nanofluid velocity is diminished. However, the temperature enhances gradually as $\overline{M}$ increases with time.
- The fluid speed and temperature of copper-water nanofluid upsurge as radiation parameters diminish.
- For Al_2O_3-water nanofluid, the velocity and temperature profile significantly increases as the heat source parameter increases with time in stable condition.
- The steady state velocity and concentration contour tend to decrease with a decrease values of K for Ag-water nanofluid but an opposite effect is realized with respect to a temperature profile.
- The velocity and temperature of the Copper-water and Ag-water nanofluid upsurges as $\overline{Pr}$ decreases. Also, the non-dimensional velocity contour of silver-water nanofluid is greater than Cu-water nanofluid and reversal effect is noticed with respect to temperature.
- The steady-state velocities of silver-water and copper-water nanofluid were upsurges with $\overline{\phi}$ but an opposite effect was observed in the case of steady-state temperature with respect to $\overline{\phi}$.
- The concentration of copper-water nanofluid is greater than the silver-water nanofluid.
- The local as well as average Nusselt number upsurges with an increment in R, m and $n$for Ag water-based nanofluid but decreases with an increase in $\overline{M}$ and K.
- For Agwater-based nanofluid, $\tau_{\overline{X}}$(local skin friction) and $\overline{\tau}$(average skin friction) coefficient against an upsurge in $R, \overline{M}, K, m$ and $n$but enhanced with a raise in varying heat flux exponent.
- The result of enhancing $K$and m to upsurge the local and average Sherwood number for Ag-water based nanofluids. However, a reverse trend is noted for $\overline{M}$.

References

Astutia, H., Srib, P. and Kaprawia, S. (2019): Natural convection of nanofluid past an accelerate vertical plate with variable wall temperature by presence of the radiation, Frontiers in Heat and Mass Transfer (FHMT), Vol.13, No.3, pp.1-8. http://dx.doi.org/10.5098/hmt.13.3

Aziz, A. and Khan, W.A (2012): Natural convective boundary layer flow of a nanofluid past a convectively heated vertical plate, International Journal of Thermal Sciences, Vol.52, pp.83-90. https://dx.doi.org/10.1016/j.ijthermalsci.2011.10.001

Brewster, M.Q. (1992): Thermal Radiative Transfer and Properties, John Wiley and Sons, New York, USA.

Chamkha, A. J., Issa, C. and Khanafer, K. (2002): Natural convection from an inclined plate embedded in a variable porosity porous medium due to solar radiation, International Journal of Thermal Sciences, Vol. 41, Issue 1, pp: 73-81. https://dx.doi.org/10.1016/S1290-0729(01)01305-9

Chamkha, A.J. and Aly, A.M. (2011): MHD free convection flow of a nanofluid past a vertical plate in the presence of heat generation or absorption effects, Chem. Eng. Comm., Vol.198, pp. 425-441. https://dx.doi.org/10.1080/00986445.2010.520232

Choi, S and Eastman, J. A. (1995): Enhancing thermal conductivity of fluids with nanoparticles Developments and Applications of Non-Newtonian Flows, FED-Vol. 231/MD-Vol.66, pp.99-105.
Das, S. and Jana, R.N. (2015): Natural convective magneto-nanofluid flow and radiative heat transfer past a moving vertical plate, Alexandria Engineering Journal, Vol.54, pp.55–64. https://dx.doi.org/10.1016/j.aej.2015.01.001
Emmanuel, O. and Lawal, J. M. (2020): Magneto hydrodynamic casson fluid Flow past a vertical plate in the presence of thermal conductivity and chemical absorption, IJSGS FUGUSAU,Vol.6, No.2, pp. 82-90. https://dx.doi.org/10.57233/ijsgs.v6i2.111
Hamilton, R. L. and Crosser, O. K. (1962): Thermal conductivity of Heterogeneous two component system, Indand Eng Chem. Fundamentals, Vol.1, No.3, pp.187-191. https://dx.doi.org/10.1021/i160003a005
Hari, R and Akhil, S. (2017): Velocity, mass and temperature analysis of gravity-driven convection nanofluid flow past an oscillating vertical plate in the presence of magnetic field in a porous medium, Applied Thermal Engineering, Vol.110, pp. 864–874. https://dx.doi.org/10.1016/j.applthermaleng.2016.08.129
https://dx.doi.org/10.2298/TSCI161012014M
Khatun, S. and Nasrin, R. (2021). Numerical modeling of Buongiorno's nanofluid on free convection: thermophoresis and Brownian effects. Journal of Naval Architecture and Marine Engineering, Vol.18, No.2, pp. 217–239. https://dx.doi.org/10.3329/jname.v18i2.54694
Krishna, M. V. and Chamkha, A. J. (2020): Hall and ion slip effects on Unsteady MHD Convective Rotating flow of Nanofluids—Application in Biomedical Engineering, Journal of the Egyptian Mathematical Society, Vol.28:1. https://dx.doi.org/10.1186/s42787-019-0065-2
Loganathan,P., Nirmal Chand, P. and Ganesan, P. (2015): Radiation effects on an unsteady MHD natural convective flow of a nanofluid past a vertical plate, Thermal science,Vol.39, No.3, pp.1037-1050. https://dx.doi.org/10.1142/S179329201350001X
Madhu, M., Kishan, N. and Chamkha, A. J. (2017): Unsteady flow of a Maxwell nanofluid over a stretching surface in the presence of magneto hydrodynamic and thermal radiation effects, Propulsion and Power Research, Vol. 6, Issue 1.pp: 31-40. https://dx.doi.org/10.1016/j.jppr.2017.01.002
Mishra, A.K., Pattnaik Mishra, S.R and N. Senapati, N. (2020): Dissipative heat energy on Cu and Al_2O_3 ethylene–glycolbased nanofluid flow over a heated semi-infinite vertical plate, Journal of Thermal Analysis and Calorimetry. https://dx.doi.org/10.1007/s10973-020-09666-z
Mondal, H., Goqo, S.P. and Sibanda, P. (2019): Effect of chemical reaction on mixed convective nanofluid flow on a vertical plate with uniform heat and mass fluxes, Int. J. of Applied mechanics and engineering, Vol.24, No.2, pp.329-342. https://dx.doi.org/10.2478/ijame-2019-0021
Mustafa, I. and Javed, T. (2019): Heat transfer in natural convection flow of nanofluid along a vertical wavy plate with variable heat flux, Thermal science, Vol.23, No.1, pp.179-190.
Narahari, M. (2018): Unsteady free convection flow past a semi-infinite vertical plate with constant heat flux in water based nanofluid, IOP Conf. Series: Materials Science and Engineering, 342: 012085. https://dx.doi.org/10.1088/1757-899X/342/1/012085
Palani, G. and Arutchelvi, A. (2018): Heat and mass transfer effects on MHD nanofluid past over an inclined plate, International journal of engineering and technology, Vol.7, No.4-10, pp. 873-879. https://dx.doi.org/10.14419/ijet.v7i4.10.26778
Parandhamaa, A., Raju, K.V.S. and Raju, M. C. (2019): MHD Casson fluid flow through a vertical plate, Journal of Computational and Applied Research in Mechanical Engineering, Vol.9, No.2, pp.343-350. https://sid.ir/paper/768378/en
Parida, B. C., Swain, B. K., and Senapati, N. (2021). Mass transfer effect on viscous dissipative MHD flow of nanofluid over a stretching sheet embedded in a porous medium. Journal of Naval Architecture and Marine Engineering, Vol.18, No. 1, pp. 73–82. https://dx.doi.org/10.3329/jname.v18i1.53380
Rajesh, V., Chamkha, A. J. and Mallesh, M.P. (2016): Transient MHD free convection flow and heat transfer of nanofluid past an impulsively started semi-infinite vertical plate, Journal of Applied Fluid Mechanics, Vol.9, No.5, pp. 2457 2467. https://dx.doi.org/10.18869/acadpub.jafm.68.236.23443
Schlichting, H. and Gersten, K. (2001): Boundary Layer Theory, Springer-Verlag, New York, USA.
Swain, B. K., Sahu, S., Ojha, K. L., and Dash, G. (2023). Heat transfer with viscous dissipation and entropy generation in a nanofluid flow through a porous medium. Journal of Naval Architecture and Marine Engineering, Vol.20, No. 2, pp. 127–142. https://dx.doi.org/10.3329/jname.v20i2.67298